

4 - Petrology

INTRODUCTION

Preliminary petrological characterization of the Lower Miocene to Lower Oligocene(?) sedimentary sequence of CRP-2/2A is aimed at detecting the most relevant features related to the evolution of a basin which previous studies have shown received discharge mainly from the adjacent region of the Transantarctic Mountains (TAM) through local polar outlet glaciers (Barrett et al., 1981; Barrett et al., 1995; Armienti et al., 1998; Bellanca et al., 1998; Smellie, 1998).

Distinctive markers for the history of the sediment transport into the basin are represented by the relative abundance of detritus coming from the crystalline basement, sandstones of the Beacon Supergroup, Ferrar dolerites and Kirkpatrick basalts and alkaline rocks from the McMurdo Volcanic Group (MVG). All these possible sources were easily detectable in the sedimentary sequence with the limited analytical techniques available during the drilling phase. The methods which were adopted include counting and identifying all clast types, microscopic examination of rock thin-sections and smear slides of sandstones, characterization of organic compounds and X-Ray Diffraction analysis of the silt and clay fractions. These methods have allowed us to reach some general conclusions which, although needing further confirmation from more detailed studies, seem to offer a coherent description of the evolution of the sedimentary pile.

Mineral ratios were measured in fast-track whole-rock samples to look for variations related to provenance. Preliminary data on tectosilicate ratios are presented in the section on X-Ray Mineralogy, and a section on Clay Mineralogy is devoted to the origin of clay minerals and their relations with possible sources and climatic evolution. The section on Organic Geochemistry deals with the content of organic matter in relation to zones of high primary productivity and reworking of detrital coal. The modal compositions of sandstone layers are discussed in a section on Sand Grains.

Granitoids of the Granite Harbour Intrusive Complex (GHIC) are dominant in the crystalline basement (Allibone et al., 1993b) and green hornblende is their most abundant mafic phase. Since this mineral is almost entirely supplied by the GHIC, it was carefully checked throughout the core (Sand Grains section). Appraisal of the variation in exposure of the source units during the erosion of the TAM, the recycling of (Cenozoic?) sedimentary units, and the input from younger volcanic rocks was undertaken by counting clasts larger than 2 mm (Basement Clast section).

Volcanic debris from the MVG may have been carried to the sedimentation site by a variety of processes, including

direct air-fall, current transport, or as debris incorporated in local glaciers discharging close to Cape Roberts. Dating of volcanic ash levels from CRP-2/2A confirms that Cenozoic volcanism in the area is older than was previously thought from data on land (Sand Grain section). The discovery of tephra layers up to 1.2 m thick, dated isotopically by the $^{40}\text{Ar}/^{39}\text{Ar}$ method, provides potentially important time markers for the region. The age obtained (21.44 ± 0.05 Ma) represents the oldest and most precise isotopic age for any tephra in the Ross Sea region (see Chronology section, Summary chapter).

BASEMENT CLASTS

The term “basement clast” is used here in a broad sense, to refer to the granule to boulder clast population which was probably derived from the pre-Tertiary basement presently exposed in the Transantarctic Mountains west of the CRP drill sites. Clast variability data describing down-core content and grain-size variations of clasts from the Miocene-Oligocene strata of CRP-2/2A are summarized in the Clast Variability section. This section will focus on a preliminary petrographical characterization of the crystalline and other basement rocks and on the most significant variations in clast type and relative proportions among the different lithological groups. Sampling, macroscopic observations and preliminary petrographical analyses were performed following the same procedure and sample management adopted for the CRP-1 core (Cape Roberts Science Team, 1998c, 1998d).

RESULTS

Petrographical and distribution pattern data were collected on 20 503 clasts. Each was described on the basis of both dimension and lithology (see Clast Variability section). The clast population is dominated by granules and fine to coarse pebbles, but also includes minor cobbles and rare boulders. The pebbles become slightly coarser and the proportion of cobbles increases down-core, particularly below *c.* 300 mbsf.

A major change in the distribution pattern of the clast types also occurs at *c.* 310 mbsf, with granitoid-dominated clasts above and mainly dolerite clasts below (Fig. 4.1). Moreover, compositional and modal data suggest a further division into seven main detrital assemblages or petrofacies (P1 to P7). The main compositional features and trends within each petrofacies are summarized below. Relevant preliminary petrographical data on granitoids and rare clasts of metamorphic rocks are also included (see Volcanic Clasts section).

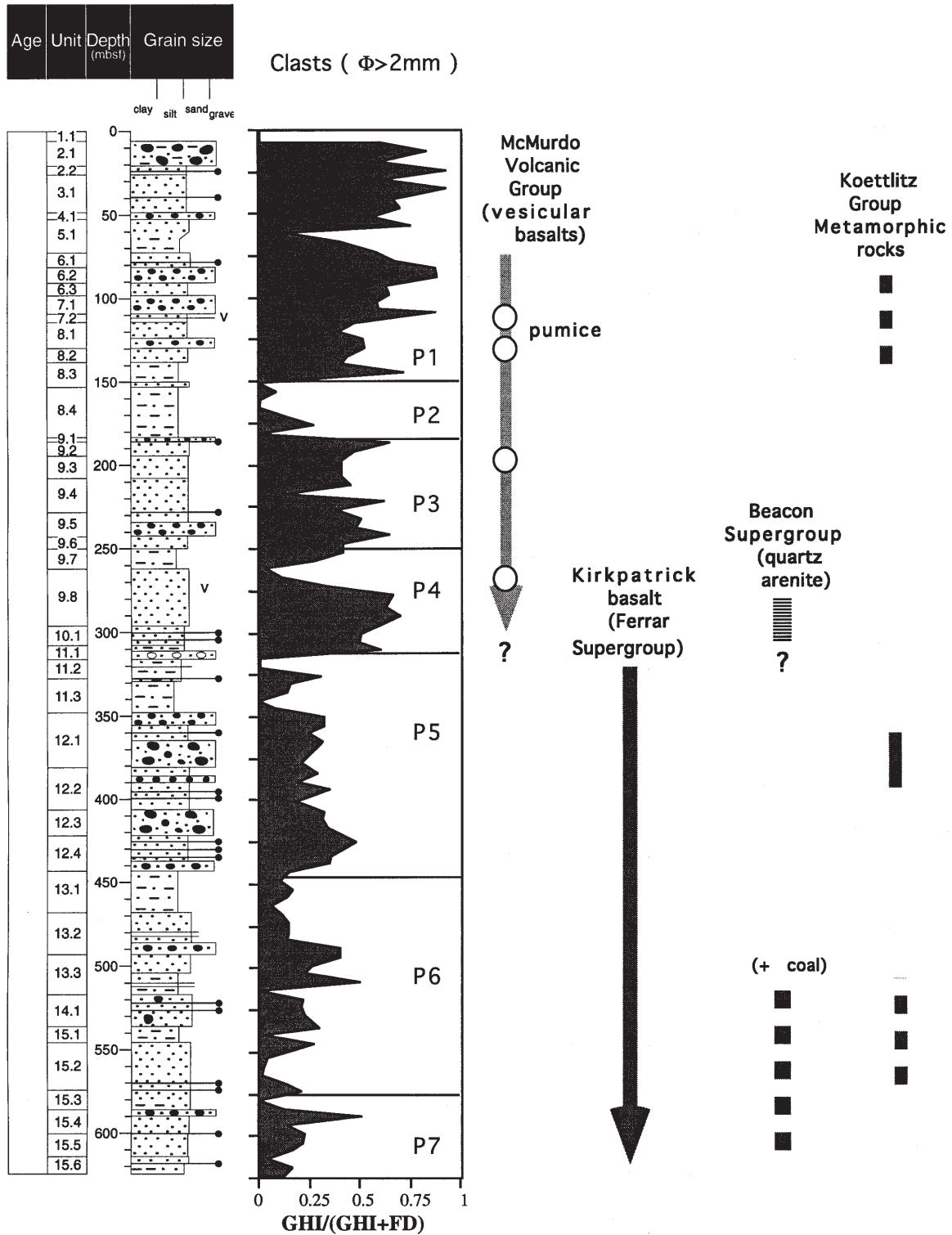


Fig. 4.1 - Proportion of major clast types (Granite Harbour Intrusive Complex, GHI, and Ferrar Supergroup dolerites, FD) plotted against depth. P1-P7 = main detrital assemblages or petrofacies. The first occurrence and distribution of minor lithologies are also shown.

P1 (26.70 to c.150 mbsf). In this petrofacies, granitoids are generally more common than dolerite (c. 80-60%), but the proportion of dolerite increases slightly with depth. Other lithologies are distinctly much less common and impersistent. They include: vesicular basalts (six occurrences: at c. 36, 77-80, 94, 122, 132 and 140-144 mbsf), pumice (forming the only clast type at 109-114 mbsf (Volcanic Clasts section),

but also occurring as a few scattered clasts at c. 101, 116, 122, 132 and 141-143 mbsf) and rare metamorphic rocks, mainly very fine-grained, thinly layered Ca-silicate rocks (at c. 79, 88, 115, 124 and 142 mbsf). A preliminary petrographical examination of P1 granitoids indicates that they consist mainly of grey medium to coarse-grained biotite monzogranite, fine- to medium-grained quartz-diorite and quartz-

monzonite, minor leucocratic biotite granite, biotite-hornblende granodiorite and rare granitic porphyry.

P2 (from c.150 to c.185 mbsf). The second assemblage is characterized by low clast concentrations, with dolerite forming the dominant lithology and a very low proportion of granitoids. The only additional rock types are represented by a few clasts of intraformational sedimentary rocks (quartz-rich sandstone, black volcanoclastic siltstone).

P3 (from c.185 to c.250 mbsf). The third petrofacies has subequal proportions of dolerite and granitoids (mainly pink biotite monzogranite), but it also includes minor vesicular basalt (at c. 178, 194, 198 mbsf) and pumice clasts (at c. 194 mbsf).

P4 (from c.250 to c.310 mbsf). At c. 250 mbsf, there is a sharp lithological and modal change. Down-core, the assemblage shows a slight increase in the proportion of granitoid clasts and a decrease in dolerite. P4 granitoids are mainly pink monzogranite, minor grey monzogranite and rare pink granitic porphyry. Vesicular basalt and sedimentary rocks are also major components; they are persistent but abundances fluctuate sharply. The sedimentary rocks are mainly intraformational clasts of grey and black siltstone, but also include a few possible Beacon Supergroup sedimentary rocks (well consolidated black siltstone with calcite veins at c. 292, and quartz arenite at c. 293 mbsf). Rare pumice clasts also occur between c. 259 and 265 mbsf.

P5 (from c.310 to c.440 mbsf). Excluding a very clast-poor section between c. 330 and 345 mbsf (Lithostratigraphical Sub-Unit 11.3), the clast assemblage in P5 is similar to P3, but contains dissimilar scarce and impersistent volcanic clasts of non-vesicular, olivine-free basalts (Jurassic Kirkpatrick basalts, see Volcanic Clasts section) and rare clasts of gneiss and Ca-silicate (at c. 360 and c. 385 mbsf). Clasts of intraformational black siltstone or sandstone are also present. Granitoid pebbles in P5 consist mainly of pink or grey biotite monzogranite but pink to orange microgranite and granitic to monzonitic porphyry are also widespread and abundant, particularly below 362 mbsf.

P6 (from c.440 to c.575 mbsf). This petrofacies is characterized by a broad peak in granitoid clast abundances at c. 475-500 mbsf (with potential for further subdivision into two sub-assemblages), and a highly variable content of non-vesicular Kirkpatrick basalts (mainly concentrated at c. 530-540 and 560-570 mbsf). Rare clasts of Ca-silicate rock and gneiss occur at c. 524, 559, 565 and 570 mbsf. Sedimentary clasts present include intraformational siltstone, minor Beacon Supergroup(?) quartz arenite (at c. 562, 566 and 573 mbsf) and dispersed coal (mainly occurring below c. 486 mbsf). P6 granitoid clasts are mainly grey to pale-pink biotite monzogranite and minor biotite-hornblende granodiorite. Pink to orange felsic porphyry is also present throughout P6.

P7 (from c.575 to 625 mbsf). This assemblage shows significant fluctuations in the proportions of granitoids (mainly grey and pink monzogrinites) and dolerite clasts, although the granitoids generally decrease down-core antithetic to the proportions of non-vesicular Kirkpatrick basalts, and a few sedimentary clasts (mainly coal and Beacon Supergroup(?) quartz arenite).

PROVENANCE

Similar to previous drill holes (MSSTS-1, CIROS-1, CRP-1) on the western edge of the Victoria Land Basin (Barrett, 1986, 1989; George, 1989; Hambrey et al., 1989; Cape Roberts Science Team, 1998a, 1998d; Talarico & Sandroni, 1998), the CRP-2/2A drill hole provides evidence of a multi-component source for the supply of granule to boulder clasts to the Tertiary sedimentary sequences in the McMurdo Sound. This varied provenance closely resembles the present-day on-shore rocks of the Transantarctic Mountains in southern Victoria Land, which include: 1) granitoid and amphibolite facies metasediments of the Early Palaeozoic Ross Orogen, 2) quartz arenites, minor black siltstones and coaly strata of the Devonian-Triassic Beacon Supergroup, 3) dolerite sills and lavas (Kirkpatrick basalt) of the Jurassic Ferrar Supergroup, and 4) alkaline volcanic rocks of the Cenozoic McMurdo Volcanic Group.

Preliminary petrographical characterization of CRP-2/2A clasts indicates that all these major geological units contributed clasts to the Miocene-Oligocene strata. As in the Quaternary-Pliocene sequence (see Introduction chapter), most of the crystalline basement pebbles were derived from the Cambro-Ordovician Granite Harbour Intrusive Complex, which is the dominant component in the local basement (Gunn & Warren, 1962; Allibone et al., 1993a, 1993b). The Miocene-Oligocene strata also contain metamorphic rocks (e.g. Ca-silicate rocks) which are known to be a common metasedimentary lithology in the amphibolite facies Koettlitz Group south of Mackay Glacier (Grindley & Warren, 1964; Findlay et al., 1984; Allibone, 1992).

Compositional and modal data indicate the presence of significant fluctuations in the relative proportions of the main lithologies (in decreasing order of abundance: granitoids, Ferrar dolerites, McMurdo Volcanic Group basalts, Kirkpatrick basalts, Beacon sedimentary rocks). In particular they point to an important lithological change at c. 310 mbsf indicating a relatively abrupt change from a mainly crystalline basement source to one dominated by Ferrar Supergroup lithologies.

The presence of significant modal and compositional variations down-core provide a clear evidence of an evolving provenance. When these data are integrated with additional provenance information obtained from concurrent geochemical, petrological and sedimentological investigations, the distinction of the seven main detrital clast assemblages has significant implications for unravelling the complex interplay between tectonic, volcanic and glaciomarine sedimentary processes during the formation of the Victoria Land Basin and uplift of the Transantarctic Mountains in Oligocene-Miocene time.

VOLCANIC CLASTS

Volcanic clasts thought to be related to activity of the Cenozoic McMurdo Volcanic Group (MVG) were collected from levels above 280 mbsf. They are generally vesicular and vary in composition from alkali basalts to

trachytes, although a few fragments of syenitic composition are also present. By contrast, below 320 mbsf, aphyric or sub-aphyric volcanic clasts become abundant. However, they are all non-vesicular basalts containing pigeonite and abundant quench-crystallized ilmenite and they are considered to be related to lava flows of Jurassic age (Kirkpatrick basalts). Volcanic clasts of both types were taken for chemical analysis to investigate their compositional variations throughout the CRP-2/2A core.

Volcanic clasts of the McMurdo Volcanic Group were examined in more detail because of their relationship with the development of the Ross Sea rift. They derive from alkaline magmas and are readily recognised by the occurrence of olivine in the groundmass of mafic lavas and strongly-coloured ferromagnesian phases (aegirine, arfvedsonite) in evolved rocks. The samples vary in size from 1 to 5 cm. Bulk sediments enriched in tephra, and hand-picked pumice fragments, were also collected for chemical investigation. Volcanic glass and mineral grains are particularly common throughout LSU 7.2 (see below), and at 193.45 and at 280.10 mbsf.

Petrographical examination of 10 representative clasts reveals the occurrence of lavas varying in composition from alkali basalt to trachyte, but alkali basalt and hawaiite are most common. Alkali basalt (CRP-2/2A 203.75 mbsf) is characterized by the presence of olivine phenocrysts, completely altered to bowlingite, and bytownitic plagioclase microphenocrysts. This clast also contains partly resorbed xenocrysts of quartz with a clinopyroxene reaction rim, a textural feature that is commonly observed in MVG basic rocks. The complete alteration of olivine in this sample may account for the scarcity of olivine in CRP-1 (Smellie, 1998) and CRP-2/2A sediments. Hawaiite and mugearite lavas mostly have fluidal textures with plagioclase and augite phenocrysts. The optically determined composition of plagioclase (labradorite) matches that of crystals derived from the MVG to the sand fraction of CRP-1 (Armienti et al., 1998). One basaltic clast shows an outer rim of tachylitic glass with small plagioclase microcrystals. The rim closely resembles opaque fragments found in the uppermost 280 m of CRP-2/2A and throughout CRP-1 (Cape Roberts Science Team, 1998b, p. 47, Fig. 12f). Felsic varieties (trachyte and syenite) differ in the degree of crystallinity. They are characterized by the occurrence of sanidine and/or anorthoclase microphenocrysts commonly accompanied by zoned green aegirine-augite microphenocrysts; fayalitic olivine also occurs in a syenite clast at 258.88 mbsf.

Parts of the sequence are rich in volcanic components (e.g. LSU 7.2, LSU 9.2 at 193.45 mbsf and LSU 9.8 at c. 280 mbsf). They contain abundant fresh, crystal-poor glass that is commonly highly vesiculated pumice. Glass is generally associated with grains of a wide variety of volcanic rocks.

LSU 7.2 - TEPHRA LAYERS

Special attention was devoted to LSU 7.2, between 108 and 114 mbsf, that contains seven main layers of tephra (Fig. 4.2). Four samples were taken at different

levels for $^{40}\text{Ar}/^{39}\text{Ar}$ isotopic dating. Individual pumice fragments from different layers were also hand-picked for whole-rock chemical analyses to establish any compositional variation.

Tephra are scattered throughout LSU 7.2. Thin beds of fine sandstone and siltstone separate pumice-rich beds. Some layers have dispersed pumice with a very variable concentration. Many of the pumice lapilli, including some in the 1.2 m-thick layer, are well rounded. The 1.2 m-thick layer and the layer at bottom of LSU 7.2 (Fig. 4.2), contain a high proportion of fine glassy tuff matrix.

Four samples were examined petrographically: Sample CRP-2/2A 111.28 mbsf is a poorly bedded, poorly sorted lapillistone formed of pumice lapilli that range in size from about 10 mm to less than 1 mm, together with 5% admixed lithic clasts. The pumice lapilli consist of colourless glass and are supported by a fine-sand matrix of quartz and feldspar fragments with abundant brown glass shards, green hornblende and pyroxene. Sponge spicules and diatoms are common.

Samples CRP-2/2A 111.77, and 112.25 mbsf (from the 1.2 m-thick bed) and CRP-2/2A 114.12 mbsf come from beds of tephra dominated by poorly sorted pumice lapilli (70-80%) set in a matrix of very fine grained vitric ash. The lapilli are almost crystal-free, highly vesiculated and colourless. The deposits also contain scattered crystals of alkali feldspar, aegirine-augite and sporadic Na-amphibole (arfvedsonite). The paucity of comagmatic plagioclase feldspar, the sporadic occurrence of angular quartz (from the basement of the volcano?) and association with anorthoclase, aegirine-augite and arfvedsonite suggest that the pumices have a peralkaline trachytic or phonolitic composition, like other rocks commonly found in MVG and in CRP-1 core (Armienti et al., 1998). Small accessory fragments (<1 mm) of altered volcanic rocks and holocrystalline trachyte are also common.

Origin of Tephra Layers in LSU 7.2

The absence of detrital sand grains, that would occur within the matrix if the layer had suffered redeposition within the basin, suggests that the 1.2 m-thick layer (Samples CRP-2/2A 111.77, 112.25 mbsf) and that at 114.12 mbsf are not reworked deposits. However, at the very top of the 1.2 m-thick bed, small pockets of silt-size crystals and brown glass suggest that it is slightly reworked or redeposited. In the remaining bulk of the layer, the proportion of ash matrix is high (20 to 30%) for a water-deposited tephra and is possibly due to the high vesiculation of pumice that made it sink as slowly as the ash. Preservation of delicate grading within these ash-rich tephra layers also argues against its redeposition after mobilisation in the sedimentary basin. Similar arguments also apply to the layer at the bottom of LSU 7.2.

Some subdivisions proposed in the 1:20 core log for the 1.2 m-thick layer, on the basis of grading and grain-size variations, could be simply linked to different settling velocity of larger particles in the water column more than to pulsation in eruptive activity. The rounded shapes of some lapilli suggest that the pumice fragments spent some time as floating rafts prior to sinking.

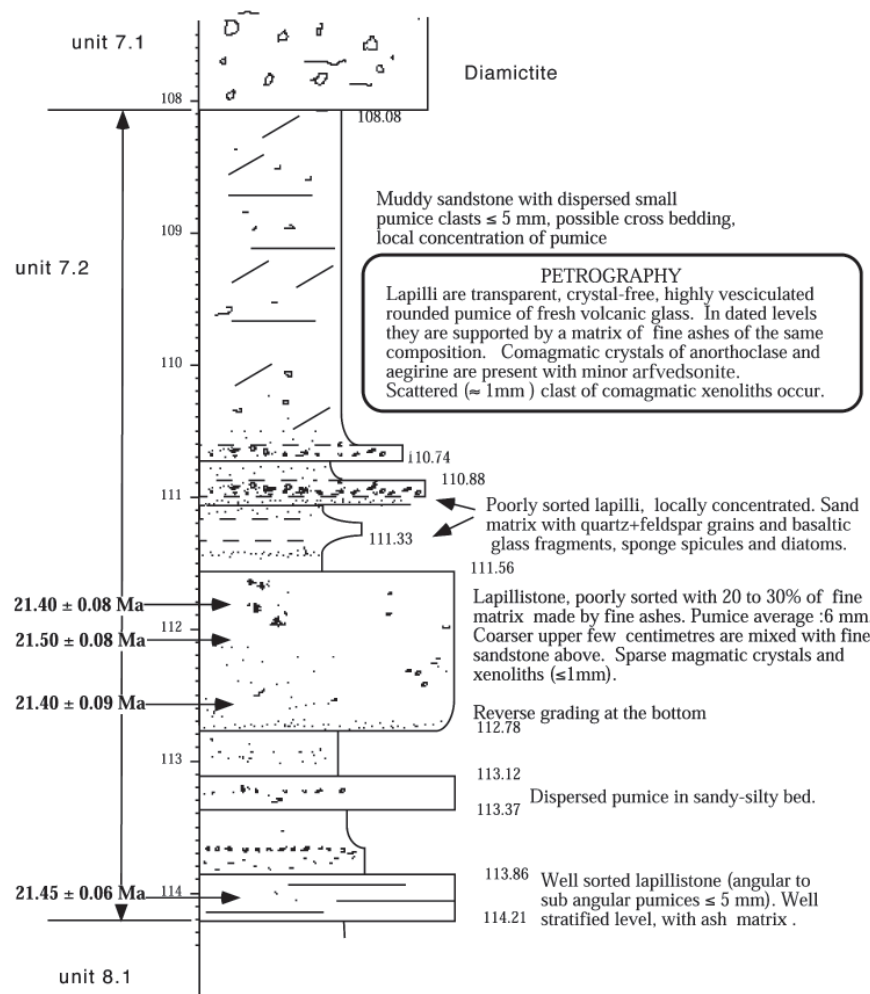


Fig. 4.2 - Stratigraphical log of ash-rich LSU 7.2, with petrographical and geochronological information.

Evaluation of the Height of Eruptive Column of the 1.2 m-Thick Layer

Calculations were performed to estimate the height of the eruptive column able to disperse pumice particles found in the 1.2 m-thick tephra layer, using a model of advection and diffusion of volcanic particles (Armienti et al., 1988; column-heights calculated by Gianni Macedonio, Osservatorio Vesuviano, Naples, Italy). A horizontal transport distance of 120 km was postulated - *i.e.* the distance to the nearest known volcanic centre on land of comparable age (Mount Morning area; Kyle, 1990). Particles were assumed to be of spherical shape and wind velocity was kept constant. Two typical sizes found at the base of the layer were taken into account: 1 mm and 2 mm, with settling velocities of 7.74 m s⁻¹ and 11.0 m s⁻¹, respectively. Larger particles may have floated longer before sinking to the sea floor and, moreover, they would require unrealistic column heights or wind speed for the assumed distance of 120 km. The results of the calculations are shown in figure 4.3, where the heights of release from an eruptive column of the two particle sizes are plotted as a function of the wind speed. Shorter travel distances imply an almost linear decrease of the column height (for a distance of 60 km we can expect approximately the same column height needed for a wind of double the speed). A

tentative estimate of column height, for a distance between 60 and 120 km and wind speed of 100 km h⁻¹, is between 33 and 17 km for 1 mm lapilli. Note that a high wind speed may constrain deposition of tephra to a narrow region focused along the plume dispersal axis. Some transport of pumice on the sea surface seems to be implied by the

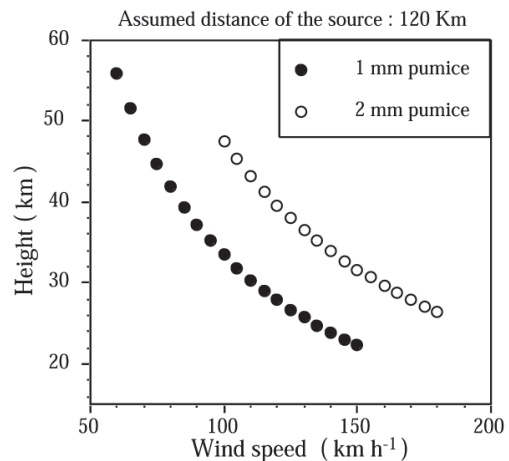


Fig. 4.3 - Effects of wind speed on the height of release required to transport pumice particles of 1 and 2 mm diameter for a distance of 120 km.

rounded shape of the pumice fragments. Moreover, the large abundance of particles of about 6 mm of diameter in the bulk of the layer suggests that a much lower column was responsible of the deposition of the tephra layer. This implies that the volcanic source was even closer than our calculations based on smaller pumice sizes suggest. An unknown volcanic centre may have been responsible for the activity, possibly within 60 km of Cape Roberts drilling site.

Age of LSU 7.2 Tephra Layers

A total of 98 single feldspar crystals were extracted from four samples from LSU 7.2, from depths between 111.58 and 114.15 mbsf (Fig. 4.2). Following neutron irradiation at Texas Agricultural and Mechanical Nuclear Science Center, samples were analyzed by W.C. McIntosh and L. Peters using the $^{40}\text{Ar}/^{39}\text{Ar}$ laser fusion method in the New Mexico Geochronology Research Laboratory at New Mexico Institute of Mining and Technology. Procedures were the same as those described by McIntosh & Chamberlin (1984). All ages were determined relative to the Fish Canyon Tuff sanidine inter-laboratory standard with an assigned age of 27.84 Ma (Deino & Potts, 1990). Of the 98 crystals analysed, ten were found to be older xenocrysts. After rejecting those and an additional four crystals which gave poor data, the remaining 84 crystals yielded precise, tightly grouped age data with high radiogenic yield, typically 99% or higher (Fig. 4.4). Mean ages calculated from analysis of those 84 crystals are as follows (all errors quoted at $\pm 2\sigma$):

CRP-2/2A-111.58-111.75	n=18	21.40 \pm 0.08 Ma
CRP-2/2A-112.19-112.34	n=11	21.50 \pm 0.07 Ma
CRP-2/2A-112.61-112.77	n=27	21.40 \pm 0.09 Ma
CRP-2/2A-114.03-114.15	n=28	21.45 \pm 0.06 Ma
CRP-2/2A-111.58-114.15 (mean)	n=84	21.44 \pm 0.05 Ma

The ages of all four samples overlap at $\pm 2\sigma$ and are considered to be analytically indistinguishable. The early Miocene mean age of 21.44 \pm 0.05 Ma is considered to be an accurate age determination for the eruption, or series of eruptions, that produced these tephra layers. There is no obvious source for the rejected much older crystals, whose ages range between 159 and 393 Ma. Their source(s) may have been of Palaeozoic age, with partial age resetting due to incorporation of the small crystals in a hot magmatic column.

SUMMARY

The study of volcanic clasts and tephra layers in the CRP-2/2A sequence allows us to suggest that:

- volcanic clasts above 280 mbsf belong to the activity of some volcanic centre of the McMurdo Volcanic Group. Volcanic clasts from below 350 mbsf are derived from Kirkpatrick basalt lava flows;
- volcanic tephra layers in LSU 7.2 (at 111.56-112.78 and 113.86-114.21 mbsf) are not reworked, and their isotopic age (21.44 \pm 0.05 Ma) is a likely age for their eruption and deposition;
- the height of the eruptive column responsible for the deposition of the tephra was probably less than 17 km. A local source is suggested, possibly within 60 km of the drilling site.

CLAY MINERALOGY

X-ray diffraction (XRD) analyses of clay minerals were performed on 29 fast-track samples distributed throughout the CRP-2 and CRP-2A cores (Tab. 4.1). After sieving the samples through a 63 μm mesh, the clay fraction was isolated from the silt fraction in large settling tubes by the Atterberg method with the settling time based

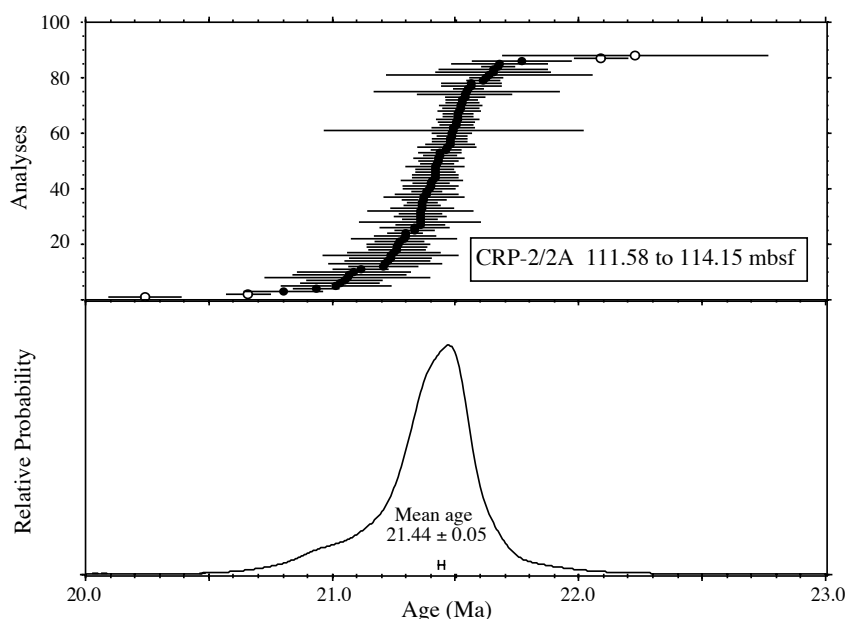


Fig. 4.4 - Probability distribution diagram of single-crystal laser-fusion analyses from CRP-2/2A-112.58-114.15 mbsf feldspars. Upper panel shows individual analyses with $\pm 1\sigma$ error bars; lower panel shows cumulative probability distribution curve. Hollow symbols denote analyses rejected from mean age calculations. (Analyses by W.C. McIntosh, New Mexico Geochronology Research Laboratory).

Tab. 4.1 - Estimates of the relative abundance of the main clay mineral groups smectite, illite, chlorite and kaolinite in the clay fraction of sediments from CRP-2/2A core.

Sample (mbsf)	Smectite	Illite	Chlorite	Kaolinite
28.90	x x x x	x x x x x x x x x x x x	x x x	x
36.24	x x x x x	x x x x x x x x x x	x x x x	x
47.41	x x x x	x x x x x x x x x x x x	x x x x	(x)
57.32	x x x x x	x x x x x x x x x x x x	x x x	x
71.13	x x x	x x x x x x x x x x x x	x x x x	x
75.60	x x x x x x	x x x x x x x x x x	x x x x	(x)
96.71	x x x x x	x x x x x x x x x x	x x x x	x
130.73	x x x x x	x x x x x x x x x x x x	x x x	x
158.38	x x x x x	x x x x x x x x x x	x x x x	x
177.89	x x x x	x x x x x x x x x x x x	x x x x	x
195.57	x x x x	x x x x x x x x x x x x	x x x x	x
215.60	x x x x x	x x x x x x x x x x x x	x x x	x
236.25	x x x x	x x x x x x x x x x	x x x x x	x
260.04	x x x	x x x x x x x x x x x x	x x x x x	x
292.09	x x x x x x x x x x	x x x x x x x	x x x	x
316.44	x x x x x x x x x x	x x x x x x x x	x x x	x
338.82	x x x x x x	x x x x x x x x x x	x x x x	x
358.24	x x x x	x x x x x x x x x x x x	x x x x	x
390.25	x x x x x	x x x x x x x x x x	x x x x	(x)
412.25	x x x x x x x x x	x x x x x x x x	x x x	x
444.78	x x x x x x x x	x x x x x x x	x x x x	x
465.06	x x x x x	x x x x x x x x x x	x x x x x x	(x)
486.19	x x x x	x x x x x x x x x x	x x x x x x	x
524.41	x x x x	x x x x x x x x x x	x x x x x x	x
543.87	x x x x	x x x x x x x x x x x x	x x x x x	x
564.58	x x x x x x	x x x x x x x x x x	x x x x	x
584.48	x x x x x x x x x x	x x x x x x x	x x x	x
604.50	x x x x x x x x x x x	x x x x x	x x x x	x
623.67	x x x x x x x x x x x x	x x x x	x x x x	x

Note: the number of crosses is proportional to the abundance of the clay minerals.

on Stoke's Law. 5-10 ml of a 50% MgCl₂ solution was added to the clay suspension (up to 5 litres) in order to charge the clay minerals and make them sink by agglomeration. Subsequently, excess ions were removed by double centrifuging in de-ionised water.

The clay fraction was then dispersed in about 15-20 ml water. The clays were mounted as texturally orientated aggregates by dropping about 1 ml of the clay suspension onto cardboard discs and evaporating the water. The cardboard discs were then mounted with double-sided adhesive tape into aluminium sample holders. The mounted clays were solvated with ethylene-glycol vapour for about 18 hrs immediately before the X-ray analyses.

The XRD measurements were conducted on a Rigaku Miniflex automated diffractometer system with CuK_α radiation (30 kV, 15 mA). The samples were X-rayed in the range 2-30 °2θ in steps of 0.01 °2θ with a measuring time of two seconds per step. The X-ray diffractograms were evaluated on an Apple Macintosh Personal Computer using the "MacDiff" software (Petschick, unpublished freeware).

The study concentrated on the presence and abundance of the main clay mineral groups smectite, illite, chlorite and kaolinite, based on the integrated areas of their basal reflections at *c.* 15-17 Å (smectite), 10 Å (illite), 7 and 3.54 Å (chlorite), and 7 and 3.57 Å (kaolinite). Only rough estimates, rather than precise percentages are given, because the separation of the clay fraction and the textural orientation of the clay aggregates on the mounts were incomplete.

In general, the clay mineral assemblages of the CRP-2/2A core are dominated by illite, with chlorite and smectite being common and kaolinite occurring in trace amounts (Tab. 4.1). Non-clay minerals, quartz, plagioclase feldspar

and K-feldspar are present in high concentrations in the clay fraction of all samples; amphibole concentrations, however, are low. Such an assemblage also dominates the lower Miocene sediments of core CRP-1 (Ehrmann, 1998b) and long intervals within the Oligocene-lower Miocene sediments of cores from CIROS-1 and MSSTS-1 (Ehrmann, 1997, 1998a).

Illite and chlorite are typical detrital clay minerals. They cannot form in the normal marine environment but are the products of physical weathering and glacial scour. Illite and chlorite are therefore typical of the recent high latitudes. They are derived particularly from crystalline rocks, such as those that are widespread on the East Antarctic craton and in the Transantarctic Mountains. Chlorite is a characteristic mineral for low-grade, chlorite-bearing metamorphic and basic rocks, but is not resistant against chemical weathering and transport. Illite tends to be derived from more acidic rocks and is relatively resistant (Biscaye, 1965; Griffin et al., 1968; Windom, 1976). Both clay minerals could also be derived from the sedimentary rocks of the Beacon Supergroup (La Prade, 1982), which overlie the basement in the western part of the Transantarctic Mountains.

In general, high smectite concentrations are mostly a product of chemical weathering and form by hydrolysis under climatic conditions between warm-humid and cold-dry, in environments characterized by very slow movement of water (Chamley, 1989). Therefore, smectite formation in the recent Antarctic environment is usually only a subordinate process. However, another source for smectite is the weathering of volcanic rocks and thus, high smectite concentrations have been reported from glacial marine sediments in areas with volcanic rocks in the hinterland

(Ehrmann et al., 1992; Ehrmann, 1998b), showing that those rocks can provide considerable amounts of smectite, even under a polar climate.

In the case of the CRP-2/2A sediments, the smectite probably is derived from a source local to McMurdo Sound, which is characterized by basaltic volcanic rocks that occur over a wide area between Ross Island and Mount Morning (McMurdo Volcanic Group). The oldest known surface samples of this area are dated at 19 Ma (Kyle, 1990). According to magnetic surveys, many more volcanic centres of similar size but unknown age exist on the present Ross Sea continental shelf, beneath the Ross Ice Shelf and the West Antarctic ice sheet (Behrendt et al., 1994, 1995), and could have contributed to the CRP-2/2A smectites. Weathering of Ferrar dolerite or Kirkpatrick basalt in the Transantarctic Mountains is a further possible origin for the smectite in the CRP-2/2A sediments.

The clay mineral assemblages in the upper *c.* 290 m of core CRP-2/2A show only minor down-core fluctuations (Tab. 4.1). Generally, illite is the dominant clay mineral with concentrations of roughly 50-60%, whereas both chlorite and smectite concentrations fluctuate probably between 15% and 25%. Such an assemblage is typical for a sediment source in the Transantarctic Mountains, where physical weathering of basement rocks and sedimentary rocks of the Beacon Supergroup provide large amounts of both illite and chlorite. Such a source therefore seems to have dominated throughout the time represented by the upper *c.* 290 m of the CRP-2/2A core.

Below *c.* 290 mbsf, the clay mineral record allows a subdivision into two major assemblages. One assemblage is the illite-dominated assemblage described above. The other assemblage is characterized by distinctly enhanced smectite concentrations but relatively low illite concentrations. Two short intervals with enhanced smectite concentrations can be identified at *c.* 290-320 mbsf and *c.* 410-450 mbsf (Tab. 4.1). In these intervals the smectite contents seem to increase to *c.* 40-45%, at the expense mainly of illite but also of chlorite. At the moment, it is not clear what caused the increase. Theoretically it could be caused by the enhanced input of smectite from a source in the McMurdo Volcanic Group to the south, either by ice or by suspension in ocean currents. Similarly, in the core from CIROS-1, two upper Oligocene intervals with high smectite concentrations were also ascribed to a southerly source (Ehrmann, 1998a). However, the investigations of the gravel and sand fractions showed no major input of volcanic components from the McMurdo Volcanic Group below *c.* 290 mbsf. A source in the Ferrar dolerites and Kirkpatrick basalts in the Transantarctic Mountains is also possible, if that source is not strongly diluted by weathering products of the crystalline basement and the sedimentary sequences of the Beacon Supergroup, which mainly provide illite and chlorite. Ferrar dolerite and Kirkpatrick basalt are constituents of the gravel and sand fraction of the sediments. Theoretically, the enhanced smectite concentrations could also indicate somewhat warmer and more humid conditions on the Antarctic continent, resulting in more intense chemical weathering, although diamictites and other glaciomarine sediments were deposited at the drill site during that time.

The biostratigraphical investigations (see Palaeontology chapter) indicate that the CRP-2/2A core penetrated into lowermost Oligocene sediments, but did not reach the Eocene/Oligocene boundary. If our rough and preliminary data on the clay mineral assemblages are correct, then they could support this biostratigraphical dating. Thus, in the lowermost part of CRP-2/2A, below 560 mbsf, the smectite concentrations steadily increase from *c.* 20% to *c.* 55%.

Just above the Eocene/Oligocene-boundary a very distinct change in the clay mineral composition from an older smectite-dominated to a younger illite-dominated assemblage is well documented in the deep-sea record of the Southern Ocean (Ehrmann & Mackensen, 1992; Ehrmann et al., 1992) and also in the core from CIROS-1 (Ehrmann, 1997, 1998a). In the deep sea, that transition can be dated to 33.7-32.7 Ma (time scale of Berggren et al., 1995). The higher smectite concentrations in the lowermost Oligocene and Eocene sediments of the CIROS-1 core and of deep-sea cores were interpreted to reflect chemical weathering under a temperate and humid climate on the Antarctic continent, when large parts of East Antarctica were probably ice-free, but several glaciers reached the coast of McMurdo Sound and icebergs calved into the sea and contributed to the glaciomarine sedimentation. However, it is also acknowledged that the smectite maximum observed in the lowermost part of the CRP2/2A core could be caused by a change in the source area.

X-RAY MINERALOGY

In order to provide a general characterization of the bulk mineralogy of pre-Pliocene sediments from CRP-2/2A, 26 "fast-track" samples were analyzed using a Rigaku Miniflex+ X-ray diffraction (XRD) system at the Crary Science and Engineering Center. The materials were analysed, and the diffraction patterns were processed with JADE 3+ software, using procedures described in the Initial Report volume for CRP-1 (Cape Roberts Science Team, 1998c, p. 84-85).

Sample locations and the minerals identified in each sample are listed in table 4.2. Quartz and plagioclase feldspars are the dominant phases in each sample, with lesser amounts of K-feldspars present in most samples. The occurrence and diversity of K-feldspars decrease down-core, however. Other minerals show low intensity peaks on the XRD patterns, suggesting low abundances, and occur discontinuously in the pre-Pliocene section; these include some expected detrital phases (illite/muscovite, augite, diopside), and other phases that are identified with less confidence and may be products of *in situ* alteration (analcime, phillipsite).

The data generated by these analyses cannot be used quantitatively to determine the abundances of the various minerals present. However, comparing the intensities of two XRD peaks (one chosen for each mineral of interest) can provide a useful qualitative indicator of the variations in relative abundances of those two phases through a stratigraphical section. The same peak area ratios have been calculated for samples from CRP-2/2A as were used

Tab. 4.2 - Minerals identified by X-ray diffraction analysis in bulk samples from CRP-2/2A.

Depth (mbsf)	Minerals Present
28.89	quartz, albite, anorthite, anorthoclase, orthoclase, microcline, augite, diopside
71.23	quartz, albite, anorthite, microcline, sanidine, orthoclase, augite, diopside
96.77	quartz, albite, anorthite, anorthoclase, microcline, augite, muscovite
130.80	quartz, albite, anorthite, anorthoclase, microcline, augite, muscovite/illite
158.48	quartz, albite, anorthite, microcline, orthoclase, diopside
177.90	quartz, albite, anorthite, microcline, sanidine, Augite, diopside, muscovite/illite
195.68	quartz, albite, anorthite, anorthoclase, microcline, sanidine, orthoclase, muscovite/illite
215.70	quartz, albite, anorthite, sanidine, microcline, muscovite
236.25	quartz, albite, anorthite, sanidine(?), orthoclase, muscovite
260.00	quartz, albite, anorthite, microcline, sanidine(?), orthoclase, muscovite
292.30	quartz, albite, anorthite, microcline, sanidine, muscovite
316.45	quartz, albite, anorthite, microcline, orthoclase, muscovite/illite, gismondine(?)
339.98	quartz, albite, anorthite, anorthoclase, microcline, orthoclase, muscovite
358.35	quartz, albite, anorthite, microcline, anorthoclase(?), muscovite, diopside
390.21	quartz, albite, anorthite, anorthoclase, muscovite/illite
412.27	quartz, albite, anorthite
444.76	quartz, albite, anorthite, microcline, orthoclase, muscovite/illite, gismondine(?)
465.04	quartz, albite, anorthite, microcline, muscovite/illite, gismondine(?)
486.32	quartz, albite, anorthite, anorthoclase(?), muscovite
507.81	quartz, albite, anorthite, muscovite/illite, gismondine(?), chabazite(?)
524.39	quartz, albite, anorthite, muscovite/illite, gismondine(?)
543.85	quartz, albite, anorthite, muscovite/illite, gismondine(?)
564.68	quartz, albite, anorthite, muscovite/illite, gismondine(?)
584.59	quartz, albite, anorthite, microcline, muscovite/illite, gismondine(?), phillipsite(?), analcime(?)
604.46	quartz, albite, anorthite, muscovite(?), gismondine(?), analcime(?)
623.63	quartz, albite, anorthite, orthoclase, muscovite/illite(?), gismondine(?)

to determine total feldspar/quartz and K-feldspar/quartz ratios for the Initial Report of CRP-1 (Cape Roberts Science Team, 1998c, p. 84-85). The resulting stratigraphical profiles of feldspar/quartz and K-feldspar/quartz peak intensity ratios are shown in figures 4.5 and 4.6, respectively.

The general structures of the feldspar/quartz ratio profile (Fig. 4.5) and the K-feldspar/quartz ratio profile (Fig. 4.6) are similar, with values decreasing down-core to relatively low and uniform values below c. 300 mbsf. One potential reason for these compositional variations is a change in sediment grain-size, since feldspar/quartz ratios tend to decrease as grain-size decreases (Blatt, 1992). Such a grain-size control does not appear to have been a major influence on these curves, however, because all of the samples were taken from the finest lithologies available: muddy fine sandstones, sandy mudstones, and the matrix of muddy to fine sandy diamictites. As a result, the grain-size of the bulk sediment analyzed does not appear to vary significantly between samples, thereby minimizing the possibility that the patterns observed in

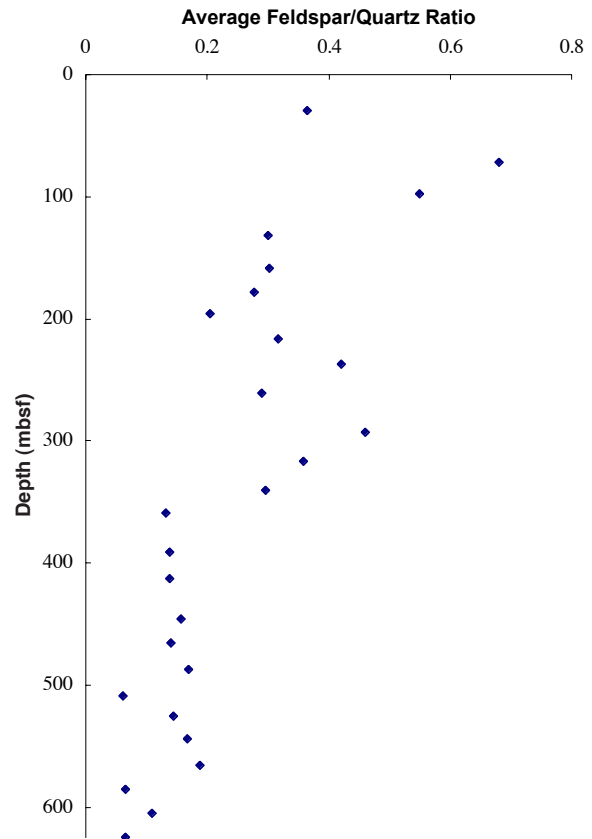


Fig. 4.5 - Stratigraphical profile of feldspar/quartz XRD peak intensity ratios for bulk sediments from CRP-2/2A. Each ratio plotted is the average of three separate peak intensity ratios. The feldspar considered in these ratios is predominantly plagioclase.

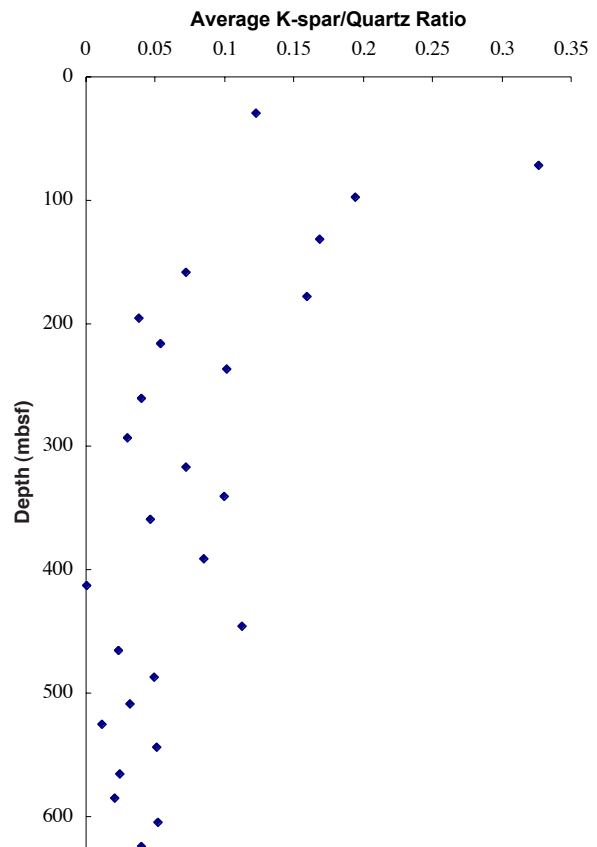


Fig. 4.6 - Stratigraphical profile of K-feldspar/quartz XRD peak intensity ratios for bulk samples from CRP-2/2A. Each ratio plotted is the average of four separate peak intensity ratios.

figures 4.5 and 4.6 are primarily a result of grain-size changes down-core.

A second possible explanation for the patterns seen in figures 4.5 and 4.6 is a change in sediment provenance during the period of deposition. The possible role of changing source contributions can be evaluated by comparing the variations in bulk mineralogy, sand fraction composition (see Sand Grains section) and coarse clast composition (see Basement Clasts section) down-core. This comparison indicates relatively consistent patterns of variation in all three compositional indicators, which aids in interpretation of the bulk mineralogical data. Above *c.* 300 mbsf, both the feldspar/quartz and the K-feldspar/quartz ratios are relatively large, although decreasing down-core. For most of this interval (to *c.* 280 mbsf), the sand fraction consistently contains components derived from the McMurdo Volcanic Group (MVG), as well as green hornblende, interpreted as being derived from the Granite Harbour Intrusive Complex (GHIC). The coarse clasts in this interval support the latter interpretation, as material derived from the GHIC is generally more abundant than other clast types. As a result, the high total plagioclase abundances and the high K-feldspar abundances relative to quartz in the bulk sediment are consistent with a sediment provenance dominated, through most of this interval, by two feldspar-rich sources (the MVG and the GHIC). At *c.* 285 - *c.* 300 mbsf, however, the absence of MVG-derived sand suggests that the GHIC are the sole source of feldspars. In addition, the predominance of plagioclase over K-feldspars in the bulk sediment is consistent with plagioclase supply from both the MVG and the GHIC, whereas K-feldspars are derived primarily from the GHIC.

Below *c.* 300 mbsf, all three compositional indicators (bulk mineralogy, sand composition, and coarse clast composition) show a consistent pattern of change. Both the total feldspar/quartz ratio and the K-feldspar/quartz ratio decrease and remain relatively uniform, green hornblende and MVG detritus are replaced by Kirkpatrick basalt and/or fine-grained dolerite in the sand fraction, and Ferrar dolerite clasts are generally more abundant than GHIC clasts. These changes all point to a shift in sediment provenance, from crystalline basement and the MVG to Beacon Supergroup sources. Recycling of quartz-rich Beacon Supergroup sedimentary rocks supplied detritus with lower total feldspar/quartz and K-feldspar/quartz ratios. That signal of Beacon sedimentary recycling is probably more evident in the bulk mineralogy (and sand grain population) than in the coarse clasts because of strength differences between Beacon sedimentary rocks and the Kirkpatrick basalt/Ferrar dolerite.

SAND GRAINS

This section describes the results of an initial investigation of the sand fraction in CRP-2A samples. It was undertaken to determine the range of sand-size mineral and lithic grains present, to estimate their relative proportions, and to provide initial information on

provenance and temporal variations. Previous studies in the area described sand grains and provenance of samples from the MSSTS-1 and CIROS-1 drill holes, both situated *c.* 80 km to the south, and CRP-1, situated about 800 m east of CRP-2/2A (Barrett et al., 1986; George, 1989; Smellie, 1998). These investigations reported a varied provenance resembling the local rocks of the Transantarctic Mountains in southern Victoria Land, including granitoid and metamorphic rocks of an Upper Precambrian-lower Palaeozoic 'basement', quartzose sedimentary rocks of the Devonian-Triassic Beacon Supergroup, sills, dykes and lavas of the Ferrar dolerite and Kirkpatrick basalt, and alkaline volcanic rocks of the Cenozoic McMurdo Volcanic Group.

METHODS

The study is based on examination of *c.* 130 unstained, covered smear slides, obtained at *c.* 5 m intervals in the CRP-2/2A core. Unlike the investigation of samples in CRP-1 (Cape Roberts Science Team, 1998b), CRP-2/2A samples were neither washed nor ground prior to smearing, thus minimising the secondary crushing of grains and avoiding unsystematic loss of biotite. However, sandstones below *c.* 500 mbsf were found to be strongly cemented and were difficult to sample in some cases without causing extensive breakage of detrital grains. The types and proportions of the major sand grains present initially were estimated visually. Seventy one samples were then selected for modal point counts, and 100 grains per sample were counted, exclusive of matrix. The point-count data are summarized in table 4.3. Both sets of modal estimates were used in the treatment of the data set, although more reliance was placed on the point-counted data for interpretations, and only those data are used in the diagrams accompanying this section. The point-counted results described here are not true detrital modes (*cf.* the Gazzi-Dickinson method; Dickinson, 1970) and the data should be regarded as qualitative.

Unlike CRP-1 samples, the CRP-2/2A samples examined are predominantly very fine- and fine-grained sandstones (60% of the sample set), with 30% of sandy siltstones/very silty sandstones and only about 10% of coarser samples (to medium sand size). Because detrital modes were not obtained on any of the siltstones or very matrix-rich very fine sandstones, the grain size of the majority of samples was more or less uniform (*i.e.* 85% of counted samples were very fine and fine sandstone), and undesirable effects of grain size variation were avoided (*cf.* Ingersoll et al., 1984; Smellie, 1998).

The different mineral and lithic grain types recognised and their inferred provenance are described in Cape Roberts Science Team (1998b, p. 46). For the visual estimates, the mineral grains were divided into simple petrographical types (*e.g.* colourless grains (quartz and feldspar), pyroxene, amphibole, volcanic glass, opaque grains), whose proportions could be determined relatively easily and reliably. For the modal counts, quartz and feldspar were separately identified, and there were also separate counts for brown and colourless glass. The opaque grain category

is a mixture of several grain lithologies, including: opaque oxide (*e.g.* (?) magnetite), extensively oxidised glass and lithic grains, feldspar densely charged with opaque 'dust', and coaly fragments.

RESULTS

The samples are dominated by colourless grains of quartz and feldspar, whose total proportion varies between 65 and 92%. The grains are variably abraded, mainly sub-angular/sub-rounded, but rounded grains are also commonly present and show a significant increase in abundance below *c.* 300 mbsf. Orthoclase is the commonest feldspar present, and other K-feldspars are minor. They are commonly charged with very fine opaque 'dust' that either gives crystals a reddish coloration or the grains are largely opaque. Plagioclase is also ubiquitous, mainly sodic in composition (albite-andesine) but accompanied by calcic plagioclase (labradorite-bytownite) and showing minor sericitic clay alteration.

Among the coloured mineral grain population, two pyroxene minerals are commonly present: 1) abraded translucent green pyroxene (augite, pigeonite and hypersthene) with prominent cleavage, a variable proportion of exsolved opaque oxide and/or fine parallel exsolution lamellae, and 2) angular grains of transparent very pale green or colourless clinopyroxene (augite). Although often petrographically distinctive, the two types grade in appearance into one another and no attempt was made to distinguish them quantitatively. They are rarely accompanied by trace amounts of titanite and aegirine or aegirine-augite. Amphibole is also ubiquitous, mainly a green to brownish green pleochroic hornblende, but including trace amounts of brown hornblende, (?)kaersutite and very rare (?)aenigmatite. Mica grains are represented by brown or rarely green biotite with a distribution mirroring that of amphibole (see below). The pyroxenes are a major component of most samples and typically form 7-20% of the mode. Amphibole varies between 0 and 4%, whereas biotite mainly occurs in trace amounts.

Volcanic glass is common above *c.* 280 mbsf, almost disappearing below that depth; it last appears in a sample at 469 mbsf. It is mainly poorly to non-vesicular, with blocky shapes and is fresh (very rarely (?)palagonite-altered) and predominantly angular; abraded glass is conspicuous in a few samples. Brown (basaltic?) and colourless (evolved - trachytic?) glass are ubiquitous; red glass is also present but less common. Glassy lapilli composed of very finely vesicular, colourless long-tube pumice are common and conspicuous in LSU 7.1 and 7.2 (note: all subsequent unit references are to lithostatigraphical sub-units), and form a thin 'layer' at *c.* 280 mbsf. The pumice is essentially identical in appearance to that forming the tephra layers in LSU 7.2 (Volcanic Clasts section).

Opaque grains are present but are very poorly characterized owing to extensive opaque oxide alteration. They are mostly sub-rounded. After quartz, feldspar and pyroxene grains, they are the next most common grain type, usually varying between 2 and 12% in the mode, and

reaching a maximum of 22%. In addition to detrital coal and (?) magnetite, grains of tachylite glass, partly glassy to holocrystalline lavas, dolerite and granitoids were also identified (although granitoids were counted as their constituent minerals; *cf.* Dickinson, 1970). The opaque grain total counts also include pyroxene and K-feldspar grains almost totally replaced by opaque oxide. Lava grains above *c.* 280 mbsf are predominantly unaltered, although grains of altered lava occur to the base of the cored sequence.

Common accessory minerals include pink garnet, zircon and sphene, and rare epidote, zeolite and detrital calcite. Silicic microfossils (diatoms and sponge spicules) are ubiquitous down to *c.* 350 mbsf, but are virtually absent below that depth in the samples examined.

Most of the sandstone samples contain less than 20% matrix or cement and some are essentially matrix-free. Cements are common and include micritic carbonate, coarser carbonate (especially in diagenetic nodules; see Diagenesis section), and (below *c.* 510 mbsf) tentatively identified gypsum and anhydrite.

MODAL VARIATIONS

Quartz (Q) contents are relatively low and variable above *c.* 100 mbsf (17-51%; Tab. 4.3). They show a saw variation down the sequence below that depth, with maxima at 190 mbsf (61-70%) and 400-425 mbsf (74-75%), and minima at 243 mbsf (38%) and 440 mbsf (49%; Tab. 4.3). Below 500 mbsf, Q contents show a steady increase, from *c.* 51 to 87%, but values apparently stabilise at *c.* 80-85% from 575 mbsf to the base of the sequence. Feldspar (F) shows a broadly antithetic variation compared with quartz. F contents are relatively high and variable above 100 mbsf (15-42%), becoming essentially constant between 100 and 500 mbsf except for several minor excursions to lower values (less than 15%) at *c.* 190-200, 300-310 and 400-425 mbsf. From 500 mbsf, F contents diminish to *c.* 8-10% at *c.* 570 mbsf, then remain roughly constant to base.

A consequence of the roughly antithetic Q and F variations is that Q/F ratios are essentially constant for a large section of the sequence, only varying between 1.7 and 2.5 between about 250 and 500 mbsf (Fig. 4.7). However, a minimum occurs between 50 and 150 mbsf, and another (less obvious) between 210 and 250 mbsf. By contrast, a striking feature of the Q/F ratios is the presence of several excursions to high Q/F values at 190-200, 290-310, 365-375 and 400-425. They correspond to peaks and troughs observed in the distribution of Q and F values. Finally, Q/F ratios show a remarkable sustained trend to much higher values (reaching 10.4) starting at *c.* 486 mbsf.

Modal data for total pyroxene (P) are very scattered (generally between 6 and 32%), possibly reflecting the low total counts (for 100 grains), but they show an obvious modal peak between 35 and 42 mbsf, corresponding to values of 20-32%. A second peak is defined at *c.* 147 mbsf (22%). 50-m averaged values suggest that P contents fluctuate only slightly downcore, but there is a significant trend to much lower values commencing at *c.* 500-550 mbsf

Tab. 4.3 - Empirical detrital modes of sand grains in CRP-2/2A sediments and sedimentary rocks. The data are based on counts of 100 grains only (excluding matrix and cement), using unstained smear slides, and they are qualitative.

Sample depth (mbsf)	Grain size	Quartz	Feldspar	Pyroxene	Amphibole	Glass	Opaque and lithic grains	Other grains	Matrix (<50) and cement (%)	Notes
8.50	poorly sorted VF SD	36	29	12	2	4	17	0	31	brown & green biotite;?hemigmatite;spicules;garnet;zircon
20.40	silty VF SD	46	26	13	1	0	13	1	38	brown biotite biot; zircon; carbonate; garnet; zeolite; spicules
26.09	poorly sorted VF(-F) SD	30	19	12	2	17	18	2	25	brown biotite; aegirine?; spicules; diatoms; zircon; sphene
26.59	F SD	51	28	15	0	1	5	0	12	epidote?
35.85	F SD	34	20	32	2	0	12	0	1	brown biotite
36.36	poorly sorted F(-M) SD	29	24	23	2	10	10	2	18	spicules
40.15	F SD	39	15	28	4	1	12	1	11	kaersutite?; muscovite?; spicules; garnet
41.77	F SD	49	21	24	0	1	5	0	1	kaersutite; epidote; garnet
46.44	F SD	42	32	11	2	5	7	1	2	kaersutite?; garnet; sphene/ carbonate
54.40	silty VF SD	23	21	17	3	16	19	1	31	brown biotite?; aegirine?; Ti-augite; spicules; diatoms; sphene
73.77	silty VF SD	17	23	9	1	31	15	4	30	hypersthene; Ti-augite; brown biotite; diatoms; spicules
79.00	poorly sorted VF SD	35	22	13	3	16	10	1	44	aegirine?; Ti-augite; spicules; diatoms
86.11	silty VF SST	22	42	17	2	7	10	0	47	kaersutite?; brown biotite
92.16	VF SST	25	26	8	1	15	23	2	28	hypersthene; brown & green biotite; garnet; spicules; diatoms; epidote?
111.09	silty VF SST	21	25	8	2	32	10	2	9	augite; spicules; garnet; diatoms; zircon; sphene; epidote
133.72	(F-)VF SST	32	24	16	0	15	11	2	12	kaersutite; diatoms; spicules; sphene; zircon
146.22	VF-F SST	44	25	21	1	4	5	0	5	kaersutite; sphene; diatoms; garnet; zircon
147.63	VF(-F) SST	46	27	22	1	0	4	0	7	Ti-augite; hypersthene; epidote; zircon; garnet
149.75	VF SST	46	34	12	1	3	4	0	11	garnet
152.87	VF SST	53	27	12	2	2	4	0	7	Ti-augite; hypersthene; sphene; garnet; zircon
155.91	VF-F SST	44	28	18	2	1	6	1	26	hypersthene; diatoms; garnet; zircon; sphene
186.42	well sorted M SST	70	21	6	0	0	3	0	0	hypersthene; sphene; zircon; garnet
187.46	well sorted M SST	61	20	11	0	0	6	2	3	hypersthene; garnet
193.46	silty VF SST	48	15	16	1	13	5	2	36	hypersthene; diatoms
200.33	silty VF SST	47	20	17	0	6	7	3	55	brown biotite; garnet; spicules; diatoms
224.46	well sorted VF SST	41	29	6	1	10	13	0	21	brown biotite; garnet; diatoms; spicules
243.44	muddy VF SST	38	23	12	0	15	9	3	43	hypersthene; kaersutite; green & brown biotite; diatoms; spicules
275.03	well sorted F- VF SST	47	27	12	0	8	6	0	7	Ti-augite; hypersthene; green & brown biotite; garnet; diatoms
280.07	well sorted F SST	48	26	7	1	9	9	0	9	brown biotite; garnet; sphene
280.32	well sorted F SST	55	21	9	0	3	11	1	4	hypersthene; brown biotite; diatoms; garnet
287.15	well sorted F SST	58	17	14	0	1	10	0	8	hypersthene; garnet; diatoms; sphene
295.20	well sorted F SST	52	29	11	1	0	7	0	13	brown biotite; spicules; diatoms
302.51	muddy-silty VF SST	53	22	17	1	0	7	0	40	Ti-augite; brown biotite; garnet
308.28	VF SST	60	15	13	0	0	12	0	10	hypersthene; kaersutite; brown biotite; zircon; garnet
310.10	VF SST	58	13	22	0	0	7	0	12	brown biotite; spicules; diatoms
318.35	well sorted VF SST	52	30	12	0	0	6	0	0	brown biotite; garnet
326.73	well sorted VF SST	62	26	6	0	0	6	0	0	kaersutite; brown biotite
359.00	F SST	61	26	9	0	0	4	0	30	garnet

Tab. 4.3 - Continued.

Sample depth (mbsf)	Grain size	Quartz	Feldspar	Pyroxene	Amphibole	Glass	Opaque and lithic grains	Other grains	Matrix (<50) and cement (%)	Notes
359.30	F SST	57	23	17	0	0	3	0	9	hypersthene;garnet; carbonate cement
364.22	F SST	67	18	11	0	0	4	0	7	hypersthene;garnet
372.77	(F-)VF SST	63	18	17	0	0	2	0	18	hypersthene;garnet;sphe
381.75	F SST	53	26	15	0	0	6	0	31	hypersthene?;brown biotite;garnet?
389.37	F-VF SST	50	28	21	0	0	1	0	29	Ti-augite;brown biotite;garnet;sphe
394.16	F SST	49	22	24	0	0	5	0	4	hypersthene?;brown biotite;sphe
399.00	VF SST	74	12	8	0	0	5	1	1	sphe
405.00	(F-)M SST	61	24	12	0	0	3	0	10	garnet
409.42	VF-F SST	57	25	10	1	0	7	0	8	brown biotite;spicules;garnet
417.26	F SST	51	28	16	0	0	5	0	21	carbonate cement
424.06	F SST	55	23	13	1	0	8	0	0	arfvedsonite?;garnet
426.96	M SST	79	11	6	0	0	4	0	0	hypersthene
435.45	F-M SST	49	27	23	0	Tr?	1	0	6	brown biotite;garnet
475.99	VF SST	59	25	12	1	Tr?	2	1	3	aegirine?;hypersthene?;brown biotite;sphe;garnet
479.18	(VF-)F SST	51	24	17	1	0	7	0	0	hypersthene;garnet
486.13	VF SST	59	15	15	2	0	8	1	17	brown&green biotite;zircon;garnet;calcite cement
495.12	VF SST	63	19	9	0	0	9	0	3	kaersutite?;garnet
503.91	sandy SILTST	49	23	23	0	0	5	0	0	kaersutite?;green biotite;sphe;garnet; abundant gypsum cement
510.07	F SST	73	17	3	0	0	7	0	6	brown biotite?;garnet;zircon; trace gypsum cement
511.42	F SST	64	9	14	0	0	13	0	9	garnet; abundant gypsum cement
516.37	F SST	68	10	11	0	0	11	0	11	garnet; abundant gypsum cement
522.98	F SST	74	12	7	0	0	7	0	51	garnet;sphe; micrite cement
528.18	(M-)F SST	65	10	12	0	0	13	0	45	hypersthene?;garnet
529.00	F SST	60	15	17	0	0	8	0	38	brown biotite
532.70	F-M SST	62	11	16	0	0	11	0	28	brown biotite;garnet; carbonate cement
535.20	VF-F SST	71	7	11	0	0	11	0	42	micrite&calcite cement
545.66	M SST	74	14	6	0	0	6	0	36	brown biotite;diatoms;garnet
552.67	F SST	77	10	4	0	0	9	0	0	garnet
556.68	VF SST	78	12	5	0	0	5	0	34	brown biotite;zircon;diatoms;spicules
570.97	M SST	87	3	3	0	0	7	0	0	garnet
596.28	F SST	71	14	2	0	0	13	0	40	brown biotite; abundant gypsum cement
601.40	F-VF SST	83	11	1	0	0	5	0	45	brown biotite;zircon;garnet; minor gypsum cement
615.74	F SST	83	8	1	0	0	8	0	12	gypsum cement

Note: owing to deformation of samples during sampling and slide preparation, matrix/cement values may be exaggerated.

*Other grains - listed in notes.

Abbreviations - mbsf - metres below sea floor; Tr - trace amount (<<1%); SD - sand; SST - sandstone; SILTST - siltstone; VF - very fine; F - fine; M - medium.

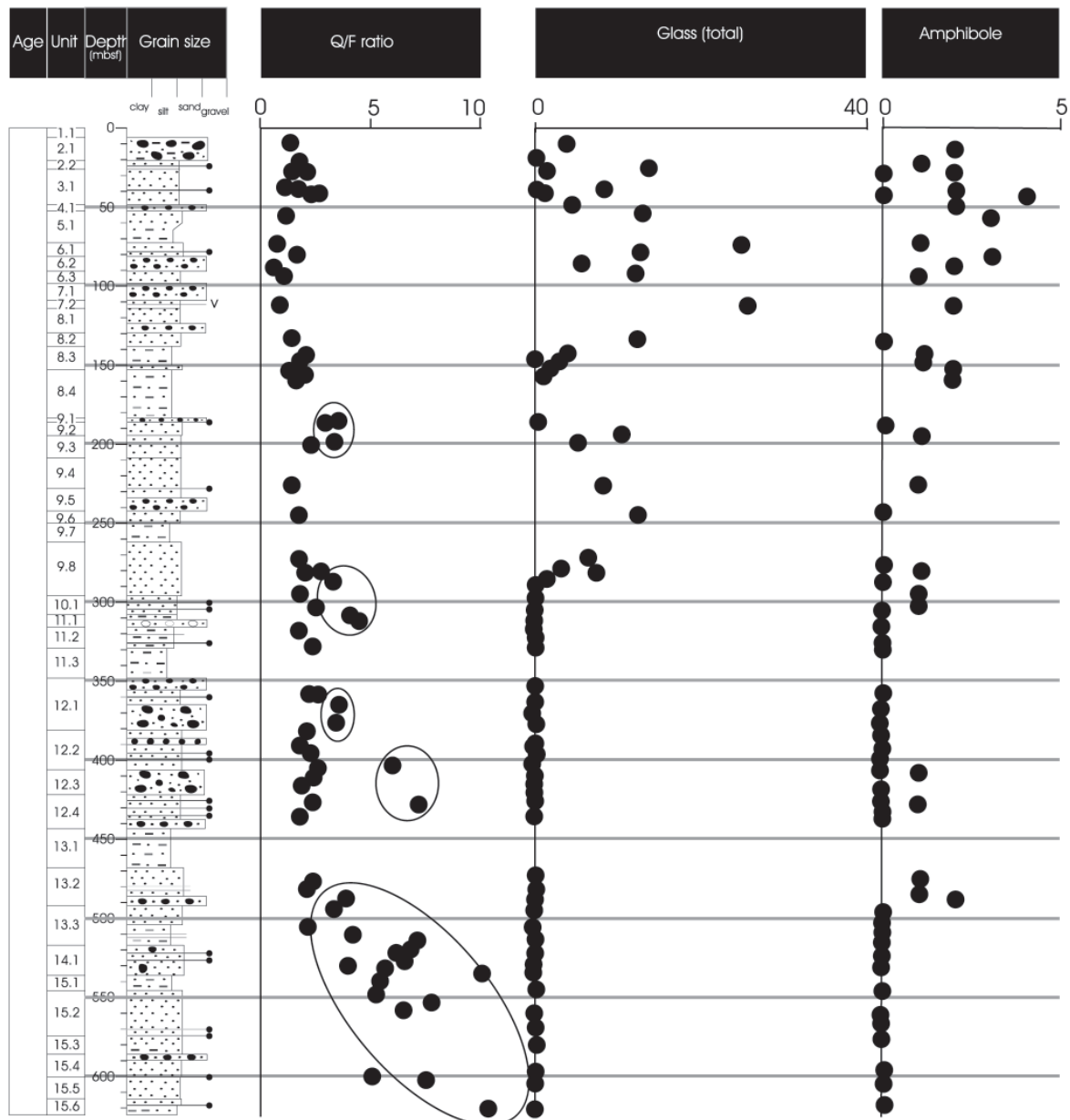


Fig. 4.7 - Summary diagram showing selected 'empirical detrital modes' for sand-grade samples from CRP-2/2A, illustrating variations of major compositional features with depth in the sequence. See text for description. Abbreviations: Q - total quartz; F - total feldspar. Samples with high Q/F ratios, believed to be dominated by Beacon-derived sand grains, are also indicated (encircled).

and decreasing to 1% at the base of the core. By contrast, amphibole shows a simple down-core trend of falling values, from *c.* 4% at 40 mbsf, becoming essentially absent below *c.* 300 mbsf (Fig. 4.7). However, amphibole is present in trace amounts in many samples to the base of the core. Biotite seems to show a similar distribution pattern to amphibole, but there are no quantified modal data since it usually occurs in trace amounts.

Modal data for glass grains show a small but distinct peak corresponding to Pliocene LSU 2.2, and two much broader peaks between 46 and 150 and 200-280 mbsf (Fig. 4.7). Below 280 mbsf, glass is practically absent, occurring only as isolated (one or two) grains in a few samples down to a depth of final appearance at 469 mbsf. Within the broad glass-rich zone at 46-150 mbsf, the glass distribution shows a strong lithofacies control. It is abundant

in beds of sandstone but absent or minor in the sandy matrices of diamictites.

Although modal values for opaque grains are very variable, at least three maxima are evident in the data set, corresponding to depths of 0-134, 200-308 and below 490 mbsf. The two upper maxima correspond closely to the two most prominent zones of peak glass abundances.

PROVENANCE

There are no grain types in the sandstone samples examined that are unique to CRP-2/2A; all are well documented from similar modal studies of samples from cores previously recovered from other sites in McMurdo Sound (MSSTS-1, CIROS-1, CRP-1; Barrett et al., 1986; George, 1989; Smellie, 1998). Similar provenances,

comprising granitoid and (volumetrically minor?) metamorphic 'basement' rocks, predominantly quartzose sandstones of the Beacon Supergroup, Ferrar dolerite and Kirkpatrick basalt, and alkaline lavas and tephra from the McMurdo Volcanic Group, are inferred for all sites.

Variations in the Q/F ratios are a clear indication of an evolving provenance. Between 625 and 500 mbsf, the sequence is characterized by variable but upward-diminishing, high Q/F ratios diagnostic of a source dominated by Beacon Supergroup sandstones (with very high Q/F ratios; Korsch, 1974). The trend to lower Q/F ratios at 500 mbsf, which are then remarkably constant between 500 and *c.* 280 mbsf (except for the three narrowly-defined Q/F 'peaks', described above; Fig. 4.7), indicates that a different lithological source has contributed to the provenance of the CRP-2/2A sandstones, which the observed grain and clast types indicate were likely 'basement' rocks (mainly granitoids and metamorphic rocks; see also Basement Clasts section). However, the intermittent presence of quartz-rich sandstones with high Q/F ratios (indicated in Fig. 4.7) suggests that Beacon Supergroup detritus temporarily dominated the local sediment supply, and these influxes are also characterised by an increased proportion of Beacon-derived rounded quartz grains (*cf.* Barrett et al., 1986; George, 1989; Smellie, 1998). Above 280 mbsf, the Q/F ratios show two 'dips' to lower ratios, 230. The locations of these features coincide with episodes of enhanced input of volcanic detritus, which diluted quartz but buffered feldspar, thus diminishing the Q/F ratios. At the end of each volcanic episode, Q/F ratios returned to values characteristic of a basement-dominated supply. Broadly comparable results are also shown by XRD analyses (see section on X-Ray Mineralogy), although the F/Q ratios used in that study (Fig. 4.5) do not clearly reproduce the pronounced ratio changes below 500 mbsf demonstrated by the sand grain modes reported here, possibly because of the fewer samples used in the XRD study.

The presence of fresh unabraded volcanic glass and tephra layers (*e.g.* at 112 mbsf; Volcanic Clasts section) is evidence for active volcanism coeval with sedimentation. The periodic influxes of volcanic debris (*e.g.* in Pliocene LSU 2.2, and at 46-150 and 200-280 mbsf) are evidence for significant volcanic episodes (*cf.* Smellie, 1998). As in CRP-1 (Armentiet al., 1998; Smellie, 1998), the volcanism was bimodal (basalt-trachyte) during all three documented episodes. The lack of a correlation between the glass-rich beds in CRP-2/2A and equivalent stratigraphical levels in CRP-1, situated only 800 m away, and the observed lithological control on the distribution of glass in CRP-2/2A indicate that input of the glass is overwhelmingly by sedimentation rather than by pyroclastic processes, which would be expected to yield a much more uniform and widespread distribution. A local volcanic source is likely, and was possibly situated within a few tens of km of the drill site. The prediction by the Cape Roberts Science Team (1998), that the glass detritus and the proportions of the compositional types may be good proxies for volcanism throughout the McMurdo Volcanic Group at any instant, is thus weakened. From the presence of fresh glass grains at 469 mbsf, volcanism was underway in the area during

early Oligocene times, at least. The sparse presence of glass between 469 and 280 mbsf suggests that the volcanic source(s) may have been relatively distant or else any glass-rich sediment bypassed the CRP-2/2A site during that depositional period. Conversely, the sudden volcanic influx at *c.* 280 mbsf indicates the inception of activity at a local volcano proximal to the drill site in late Oligocene times. It is speculated that the same volcano may have been responsible for the volcanic episode recorded by high glass abundances at 46-150 mbsf, which also probably erupted the multiple pumice layers in LSU 7.2, dated by W.C. McIntosh as 21.4 Ma (Early Miocene; see Volcanic Clasts section).

ORGANIC GEOCHEMISTRY

Some basic organic geochemical measurements were undertaken as part of the initial core characterization effort and to provide preliminary information regarding organic matter provenance, as well as the environments of deposition and early diagenesis. This effort comprised measurements of the C and N contents of 70 whole-rock samples and examination of some solvent-soluble organic matter extracted from one sample.

METHODS

Samples were collected at 5-10 m intervals and were intended to be representative of the major lithologies penetrated by CRP-2/2A. The sampling was biased to sediments and rocks with finer grain-sizes and well-preserved laminations. Although efforts were made to sample only the matrix of the diamictite and conglomerate units, some granule and pebble-sized clasts were included. An "oily overprint" was noted in the core logs at a number of intervals below 500 mbsf. Several of these intervals were sampled and one (CRP-2A-523.45-523.48) was selected for preliminary examination of solvent-soluble organic matter in the Cray Science and Engineering Center at McMurdo Station.

All samples, with the exception of CRP-2A-523.45-523.48, were freeze-dried to remove excess water, ground and homogenized in a Spex 8000 Mixer/Mill, and stored in 15 ml glass vials. All glassware used in sample preparation was cleaned with a commercial detergent followed by sequential rinses with 1% hydrochloric acid, methanol (Baker HPLC Solvent, lot J12293), and dichloromethane (Fisher Scientific, GC Resolv, lot 962656). Three sets of elemental analyses (Tab. 4.4) were performed using a Carlo-Erba NA 1500 analyzer and acetanilide as a standard: 1) total carbon (TC) and total nitrogen (TN) measurements were made on whole-rock samples, 2) total organic carbon (TOC_{LT}) was measured using the low-temperature vapour acidification technique outlined by Hedges & Stern (1984), and 3) total organic carbon (TOC_{HT}) was also measured using a high-temperature vapour acidification technique. The high temperature acidification was performed by placing a known mass of the powdered whole-rock samples in silver capsules. The capsules were then loaded in holes that had been drilled in

Tab. 4.4 - Values of total carbon (TC), total organic carbon determined by low temperature vapour acidification (TOC_{LT}), total organic carbon determined by high temperature vapour acidification (TOC_{HT}), and total nitrogen (TN) measured from samples of the CRP-1 core.

Sample	%TC	% TOC_{LT}	% TOC_{HT}	%TN	$\text{TOC}_{\text{HT}}/\text{TN}$
2-6.00-6.02	0.19± 0.02	0.18±0.01	0.092±0.003	0.007±0.001	12
2-9.85-9.87	0.28± 0.02	0.21±0.01	0.13±0.01	0.010±0.001	14
2-15.09-15.11	0.18±0.01	0.16±0.01	0.077±0.002	0.008±0.001	10
2-20.02-20.04	0.44±0.04	0.28±0.01	0.19±0.01	0.015±0.002	12
2-24.28-24.30	0.089±0.007	0.12±0.01	0.051±0.002	0.0068±0.0009	7
2-26.55-26.57	0.077±0.006	0.14±0.01	0.0087± 0.0002	0.0068±0.0009	1
2-31.41-31.43	0.20±0.02	0.26±0.01	0.17±0.01	0.016±0.002	10
2-37.42-37.44	0.25±0.02	0.22±0.01	0.14±0.01	0.016±0.002	9
2-40.42-40.44	0.21±0.02	0.20±0.01	0.13±0.01	0.012±0.002	11
2-45.04-45.06	0.26±0.02	0.25±0.01	0.30±0.01	0.018±0.002	17
2-50.15-50.17	0.15±0.01	0.16±0.01	0.12±0.01	0.012±0.002	10
2-55.10-55.12	0.29±0.02	0.19±0.01	0.15±0.01	0.014±0.002	10
2A-55.32-55.34	0.20±0.02	0.25±0.01	0.17±0.01	0.019±0.003	9
2A-67.85-67.87	0.22±0.02	0.24±0.01	0.16±0.01	0.018±0.002	9
2A-77.06-77.08	0.11±0.01	0.15±0.01	0.1±0.01	0.009±0.001	11
2A-86.43-86.45	0.11±0.01	0.13±0.01	0.097±0.01	0.010±0.001	10
2A-96.29-96.31	0.22±0.02	0.26±0.01	0.20±0.01	0.021±0.003	10
2A-107.48-107.50	0.18±0.01	0.22±0.01	0.14±0.01	0.018±0.002	8
2A-113.63-113.65	0.26±0.02	0.32±0.02	0.22±0.01	0.035±0.005	6
2A-118.74-118.76	0.19±0.02	0.25±0.01	0.17±0.01	0.017±0.002	10
2A-128.10-128.12	2.90±0.23	0.19±0.01	0.15±0.01	0.010±0.001	15
2A-135.88-135.90	0.16±0.01	0.12±0.01	0.14±0.01	0.014±0.002	10
2A-149.58-149.60	0.37±0.03	0.24±0.01	0.17±0.01	0.015±0.002	12
2A-150.97-150.99	0.77±0.06	0.26±0.01	0.18±0.01	0.016±0.002	12
2A-155.45-155.47	0.093±0.007	0.14±0.01	0.08±0.01	0.0056±0.0008	14
2A-164.95-164.97	0.34±0.03	0.31±0.02	0.24±0.01	0.021±0.003	11
2A-173.32-173.34	0.29±0.02	0.34±0.02	0.27±0.01	0.024±0.003	11
2A-176.75-176.77	0.31±0.02	0.34±0.02	0.28±0.01	0.027±0.004	10
2A-184.45-184.47	0.25±0.02	0.18±0.01	0.12±0.01	0.011±0.002	11
2A-192.44-192.46	0.11±0.01	0.12±0.01	0.075±0.003	0.0069±0.0009	11
2A-198.50-198.52	0.27±0.02	0.18±0.01	0.14±0.01	0.012±0.002	11
2A-206.82-206.84	0.37±0.03	0.22±0.01	0.15±0.01	0.014±0.002	11
2A-221.31-221.33	2.23±0.18	0.32±0.01	0.18±0.01	0.017±0.002	10
2A-226.67-226.69	0.29±0.02	0.30±0.01	0.18±0.01	0.019±0.003	9
2A-238.53-238.55	0.33±0.03	0.39±0.01	0.25±0.01	0.023±0.003	11
2A-245.34-245.36	0.35±0.03	0.38±0.01	0.22±0.01	0.027±0.004	8
2A-255.92-255.94	0.68±0.05	0.70±0.02	0.53±0.02	0.061±0.008	9
2A-270.03-270.05	0.20±0.02	0.31±0.01	0.17±0.01	0.022±0.003	8
2A-277.43-277.45	0.12±0.01	0.21±0.01	0.097±0.003	0.008±0.001	12
2A-287.11-287.13	0.15±0.01	0.23±0.01	0.12±0.01	0.008±0.001	16
2A-295.09-295.11	0.11±0.01	0.23±0.01	0.093±0.003	0.0066±0.0009	14
2A-296.83-296.85	0.93±0.07	0.26±0.01	0.14±0.01	0.015±0.002	9
2A-304.98-305.00	0.37±0.03	0.32±0.01	0.21±0.01	0.013±0.002	16
2A-314.24-314.26	0.65±0.05	0.35±0.01	0.25±0.01	0.017±0.002	15
2A-317.59-317.61	0.65±0.05	0.67±0.02	0.53±0.02	0.041±0.006	13
2A-321.59-321.61	0.58±0.05	0.29±0.01	0.19±0.01	0.010±0.001	19
2A-325.84-325.86	0.53±0.04	0.27±0.01	0.17±0.01	0.008±0.001	21
2A-337.40-337.42	1.02±0.08	0.33±0.01	0.21±0.01	0.016±0.002	13
2A-347.70-347.72	0.98±0.08	0.48±0.02	0.34±0.01	0.027±0.004	13
2A-358.09-358.11	0.58±0.05	0.45±0.01	0.34±0.01	0.024±0.003	14
2A-359.54-359.56	0.64±0.05	0.56±0.02	0.49±0.02	0.018±0.002	27
2A-370.37-370.39	0.72±0.06	0.33±0.01	0.23±0.01	0.012±0.002	19
2A-382.00-382.02	0.34±0.03	0.39±0.01	0.28±0.01	0.017±0.002	16
2A-390.38-390.40	0.47±0.04	0.56±0.02	0.39±0.01	0.026±0.004	15
2A-404.01-404.03	0.34±0.03	0.28±0.01	0.21±0.01	0.008±0.001	26
2A-412.56-412.58	0.42±0.03	0.42±0.01	0.31±0.01	0.018±0.002	17
2A-426.36-426.38	0.28±0.02	0.35±0.01	0.23±0.01	0.009±0.001	26
2A-437.73-437.75	0.49±0.04	0.32±0.01	0.21±0.01	0.015±0.002	14
2A-450.26-450.28	1.10±0.09	0.49±0.02	0.38±0.01	0.029±0.004	13
2A-459.04-459.06	0.61±0.05	0.66±0.02	0.54±0.02	0.045±0.006	12
2A-465.49-465.51	0.59±0.05	0.56±0.02	0.42±0.02	0.041±0.006	10
2A-467.51-467.53	2.02±0.16	0.47±0.02	0.36±0.01	0.027±0.004	13
2A-477.34-477.36	0.46±0.04	0.32±0.01	0.21±0.01	0.017±0.002	13
2A-481.29-481.31	0.58±0.05	0.41±0.01	0.26±0.01	0.020±0.003	13
2A-486.90-486.92	0.47±0.04	0.31±0.01	0.17±0.01	0.014±0.002	12
2A-498.72-498.74	0.072±0.006	0.16±0.01	0.04±0.01	0.008±0.001	5
2A-500.42-500.44	0.18±0.01	0.26±0.01	0.14±0.01	0.009±0.001	16
2A-523.45-523.47	0.75±0.06	0.59±0.04	0.37±0.02	0.021±0.003	18
2A-583.46-583.48	0.56±0.04	0.60±0.04	0.39±0.02	0.026±0.004	15
2A-623.21-623.23	0.62±0.05	0.65±0.04	0.44±0.03	0.023±0.003	19

a 25 mm section of 25 mm teflon rod. Each section of teflon rod could accommodate three capsules. The teflon rod and capsules were placed inside a 15 ml wide-mouth teflon bottle with 1–2 ml of concentrated HCl acid. The teflon containers were sealed with a screw closure, loaded into a stainless steel pressure vessel and placed in an oven at 150°C for 12 hours. The samples were removed after the pressure vessel had cooled and placed in a oven to dry at 55°C.

Only C and N data are reported here. The Carlo-Erba NA1500 did not function properly during the project period and whole-rock C, N and S data from all samples will be reported in the Scientific Results volume.

Sample CRP-2A-523.45–523.48 was crushed in the SPEX 8000 mixer/mill, weighed and placed in a cellulose extraction thimble. The sample was extracted for 24 hours using an azeotropic mixture of toluene (Fisher Scientific Optima, lot 962474) and methanol in a Soxhlet apparatus. The sample was then extracted for an additional 24 hours using dichloromethane. Whereas the methanol/toluene solution changed from colourless to light yellow over the course of the extraction, the dichloromethane remained colourless throughout the 24 hour extraction. The methanol/toluene solution was placed in a separating funnel and a hydrophobic phase was isolated using water that had been purified in a Barnstead 4-stage purification system. The aqueous phase was transferred to another separating funnel where a second hydrophobic phase was isolated using the dichloromethane solution obtained in the second extraction. The hydrophobic phases were evaporated to dryness under partial vacuum using a rotary evaporator. The resulting liquid was transferred to a 1 ml glass vial using dichloromethane and dried to a constant mass. This C_{15+} fraction was analyzed on a Hewlett-Packard 5890 gas chromatograph equipped with a J&W Scientific fused silica capillary column (30 m x 0.32 mm) coated with DB-5 (0.25 μ m film thickness). The flame ionization detector and injector were regulated by thermostat to 300°C, whereas the oven temperature was controlled at 38°C for 3 minutes followed by an increase to 290°C at 4°C/minute and isothermal conditions for an additional 60 minutes.

RESULTS AND DISCUSSION

TOC values obtained from the CRP-2/2A core are low. Only ten of the TOC_{LT} and three of the TOC_{HT} measurements obtained exceed 0.5% (Tab. 4.4). Although the precision of the measurements is quite good there is clearly a slight problem with accuracy: a number of the samples have TOC_{LT} values that exceed the TC values by amounts in excess of the assigned errors. The problem is most pronounced in samples with very low TOC and TC values (Tab. 4.4). Two of intervals with the highest TOC values correspond to zones with abundant biogenic sediment: 1) a zone containing abundant diatoms centred on 250 mbsf, and 2) a zone containing abundant diatoms and calcareous nannofossils centred on 460 mbsf (Fig. 4.8). The correlation between higher TOC values and greater amounts of biogenic debris is not universal, however. A number of zones with abundant biogenic sediment do not exhibit elevated TOC values; most notable among these

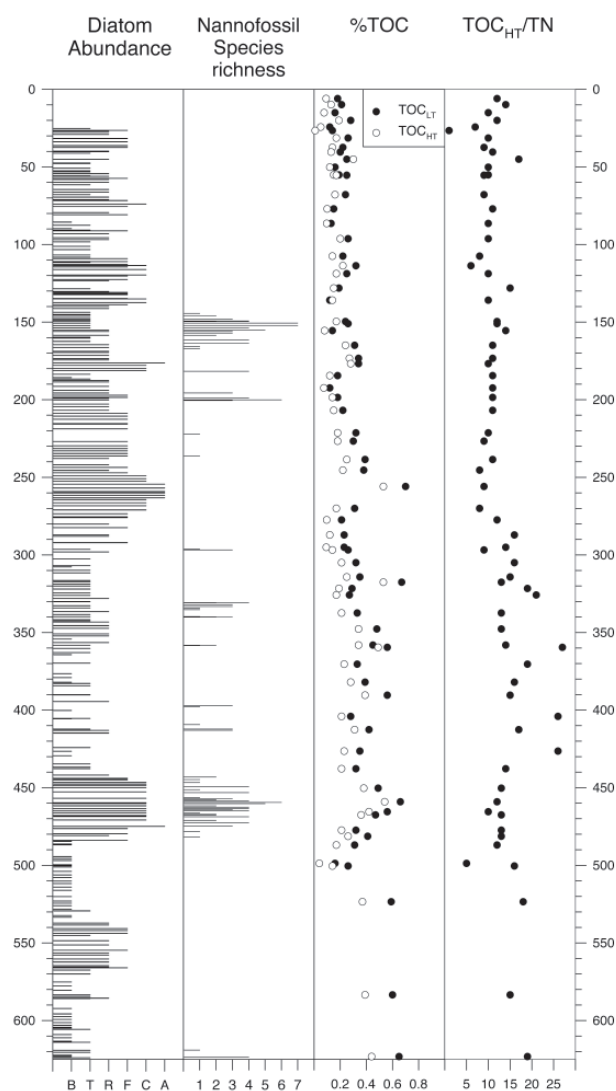


Fig. 4.8 - Comparison of values of total organic carbon determined using low temperature (TOC_{LT}) and high temperature (TOC_{HT}) vapour acidification, and TOC_{HT}/TN richness compared with the abundance of diatoms, and the nannofossil species richness of the CRP-2/2A core.

are the zones of high diatom abundance in the upper 150 m of CRP-2/2A (Fig. 4.8). Although TOC values of samples obtained from below 300 mbsf are, in general, higher than those obtained at more shallow depths (Tab. 4.4, Fig. 4.8), the slight decrease in TOC values up-section does not correspond to a similar decrease in the amount of biogenic debris.

TOC:TN ratios are high throughout the section. Organic matter with TOC:TN ratios significantly greater than 10 is derived largely from land plants and coals, whereas aquatic organisms have much lower TOC:TN ratios (Bordovskiy, 1965). The high TOC:TN ratios observed in the CRP-2/2A core are strong evidence that the preserved organic matter comprises a mixture of detrital coal and aquatic organic matter. The TOC:TN ratios decrease slightly in the high TOC sections observed at 250 mbsf and 460 mbsf and are interpreted as evidence that the preservation of greater amounts of organic carbon is related to the greater abundances of biogenic debris in these sediments and

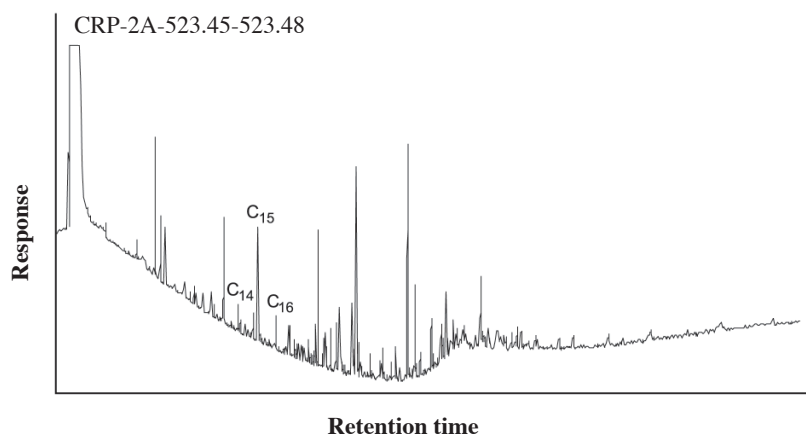


Fig. 4.9 - Chromatogram of solvent-soluble organic matter obtained from Sample CRP-2A-523.45-523.48. The peaks labeled C₁₄, C₁₅, and C₁₆ have been tentatively identified as the alkanes n-tetradecane, n-pentadecane, and n-hexadecane.

rocks. On the other hand, the TOC:TN ratios of samples obtained from below 300 mbsf are elevated slightly relative to those in the upper portion of the core, and are evidence that detrital coal is more abundant in the lower portion of the core than it is from 0 to 300 mbsf.

Two types of TOC measurements were undertaken to assess the contribution of refractory carbonate phases to the carbon content of the rocks. Although the results from the CRP-1 core were imprecise (Cape Roberts Science Team, 1998c; p. 87), no apparent difference between TOC and TC was observed. Later work established the presence of siderite in samples from the CRP-1 core (Baker & Fielding, 1998). Siderite is a refractory carbonate phase that requires months to dissolve when subjected to low temperature acidification (Rosenbaum & Shepard, 1986; p. 1148). The high-temperature vapour acidification technique was developed in an attempt to quantify the abundances of labile carbonate (largely calcite) and refractory carbonate in the CRP-2/2A core. A few samples contain significant amounts of labile carbonate reflecting the presence of the calcite-cemented concretions and layers observed in the core. Examples include CRP-2A-221.31-221.33, a rock that has a TC value of 2.2%, whereas the TOC_{LT} value is only 0.32%. With one exception, the values of TOC_{LT} are significantly higher than the values of TOC_{HT} for identical samples. If the different values of TOC_{LT} and TOC_{HT} are caused by the presence of siderite or other refractory carbonate phases, then one can calculate

the amounts of labile carbonate and refractory carbonate present by difference. The relationship between the TOC_{LT} and TOC_{HT} values is evidence that siderite is present in the CRP-2/2A core and, combined with the low TOC values, is evidence that the diagenetic environment at the drill site was largely post-oxic (Berner, 1981).

Sample CRP-2A-523.45-523.48 did not fluoresce under ultraviolet light. It did, however, yield a small amount of bitumen. That sample, comprising 36.60 g of sand and shale, produced 3.6 mg of bitumen for a bitumen ratio of 27 mg bitumen/g organic carbon. Although the amount of bitumen recovered is small, it is significantly larger than the amounts recovered during processing of CRP-1 core (Kettler, 1998). A chromatogram of the total extract (Fig. 4.9) has a number of large peaks and a relatively small unresolved complex mixture (UCM). Interpretation of the chromatogram is complicated by a tailing solvent peak. The alkane hydrocarbons n-tetradecane (n-C₁₄), n-pentadecane (n-C₁₅), and n-hexadecane (n-C₁₆) are tentatively identified by comparison of retention times with a standard mixture. The small size of the UCM and the abundance of compounds with apparently lower molecular weights than n-C₁₅, are evidence that the bitumen has not been severely degraded by microbial activity or water-washing. The apparent predominance of odd-numbered alkanes over the even-numbered alkanes (Fig. 4.9) is evidence that this bitumen has a low thermal maturity.